Eur. Phys. J. C (2016) 76:202
DOI 10.1140/epjc/s10052-016-4035-7

THE EUROPEAN PHYSICAL JOURNAL C

Regular Article - Theoretical Physics

Dynamical approach to MPI in W+dijet and Z+dijet production within the PYTHIA event generator

B. Blok[1,a], **P. Gunnellini**[2]

[1] Department of Physics, Technion-Israel Institute of Technology, Haifa, Israel
[2] Deutsches Elektronen-Synchrotron (DESY), Notkestraße 85, 22761 Hamburg, Germany

Received: 27 October 2015 / Accepted: 29 March 2016 / Published online: 13 April 2016

Abstract The new numerical approach that includes $1 \otimes 2$ mechanisms is applied to double parton scattering (DPS) in W+dijet and Z+dijet final-state production in proton–proton collisions at the LHC. By using the underlying event (UE) simulation from a PYTHIA 8.205 tune extracted in hadronic events, we show that, like in the case of a four-jet final state, the inclusion of $1 \otimes 2$ mechanisms improves the description of experimental data measured at 7 TeV. The analysis is based on applying an event-by-event reweighting factor to a standard PYTHIA 8.205 sample, by using the theoretical value of $\sigma_{\rm eff}$, which includes corrections due to $1 \otimes 2$ mechanisms. In addition, predictions for proton–proton collisions at a center-of-mass energy of 13 TeV are shown for DPS-sensitive observables. The relevant code, used for this analysis, is publicly available at the following link: http://desy.de/~gunnep/SigmaEffectiveDependence/.

1 Introduction

Hard multiple parton interactions (MPI) play an important role in the description of inelastic proton–proton (pp) collisions at high center-of-mass energies. Starting from the 80s [1–5] until the last decade [6–33], extensive theoretical studies have been performed. Significant progress was made on the simulation of multi-parton collisions in Monte Carlo (MC) event generators [28–31,34,35,35–40]. Multiple parton interactions can serve as a probe for non-perturbative correlations between partons in the nucleon wave function and are crucial for determining the structure of the underlying event (UE) at Large Hadron Collider (LHC) energies. Moreover, they constitute an important background for new physics searches at the LHC. A large number of experimental measurements has been released at the Tevatron [41–43] and at the LHC [44–51], showing a clear evidence of MPI at both soft and hard scales. The latter case is usually referred to as "Double Parton Scattering" (DPS), which involves two hard scatterings within the same hadronic collision. The cross section of such an event is generally expressed in terms of $\sigma_{\rm eff}$ [1–27,32]. In the so-called "mean-field approximation", the cross section $\sigma_{\rm eff}$ is the effective area which measures the transverse distribution of partons inside the colliding hadrons and their overlap in a collision.

Recently, a new approach based on perturbative Quantum Chromodynamics (pQCD) has been developed [22–25] for describing MPI. Its main ingredients are listed in the following:

- the MPI cross sections are expressed through new objects, namely double generalized parton distributions ($\rm GPD_2$);
- besides the conventional mean-field parton model approach to MPI, represented by the so-called $2 \otimes 2$ mechanism (see Fig. 1 left), an additional $1 \otimes 2$ mechanism (see Fig. 1 right) is included. In this mechanism, which can be calculated in pQCD, a parton from one of the nucleons splits at some hard scale and creates two hard partons that participate in MPI. This mechanism leads to a significant transverse-scale dependence of the MPI cross sections;
- the contribution of the $2 \otimes 2$ mechanism to $\rm GPD_2$ is calculated in a mean-field approximation with model-independent parameters.

This new formalism in pp collisions at LHC energies has been implemented in the simulation of MPI [52] for four-jet final states. The new PYTHIA 8 approach has been developed by including a dynamic $\sigma_{\rm eff}$ calculation and has two basic differences from the conventional PYTHIA MPI simulation [37]. On the one hand, the MPI cross section is calculated in mean-field approach by using the factorization property of $\rm GPD_2$, which connects them to the more conventional one-parton GPD, which have been measured at HERA and parameterized in [19–22]. On the other hand, corrections due to $1 \otimes 2$

[a] e-mail: blok@physics.technion.ac.il

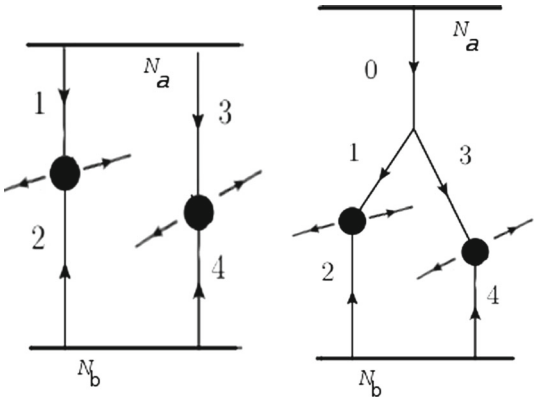

Fig. 1 Sketch of the two considered MPI mechanisms: $2 \otimes 2$ (*left*) and $1 \otimes 2$ (*right*) mechanism

mechanisms are implemented by solving nonlinear pQCD evolution equations [24,25]. The value of σ_{eff} is obtained according to

$$\sigma_{\text{eff}} = \frac{\sigma_{\text{eff}}^{(0)}}{1+R}, \tag{1}$$

where $\sigma_{\text{eff}}^{(0)}$ is the effective cross section in the mean-field approach calculated in a model-independent way, and $R(Q_1^2, Q_2^2, Q_0^2)$ is calculated by solving iteratively the non-linear evolution equation, as explained in detail in [24,25]. The two scales Q_1, Q_2 are the transverse scales of the two hardest dijet systems produced within the same pp collision, while $Q_0^2 = 0.5$–1 GeV^2 is the scale which divides soft and hard processes in the MPI formalism [25]. In such an approach, results obtained for MPI cross sections are model independent, and do not need additional fit parameters for characterizing the MPI. It has been shown [52] that the new formalism implemented in PYTHIA 8—called in [52] and hereafter "UE Tune Dynamic σ_{eff}"—leads to a consistent description of both soft and hard MPI in four-jet final states.

Furthermore, there is no problem of double counting between $1 \otimes 2$ and $2 \otimes 2$ mechanisms. Indeed, at a scale Q_0, the factorization of initial GPD_2 into a product of two one-particle GPD_1 holds by assumption. The consequent evolution from the scale Q_0 evidently does not mix the $1 \otimes 2$ and $2 \otimes 2$ contributions.[1] Note that the transverse scale $\boldsymbol{\delta}$ at which the $1 \otimes 2$ split occurs is $Q_{1,2} \gg \boldsymbol{\delta} \gg Q_0$.

The aim of this paper is to extend the approach of [52] to the study of MPI in W+dijet and Z+dijet final states. Various predictions are compared to experimental data on W+dijet (hereafter referred to as **Wjj**) [44,45] and inclusive Z production [48] at $\sqrt{s} = 7$ TeV. The former channel is sensitive to DPS contributions, while observables affected by soft MPI are measured in the latter. Predictions on Z+dijet (hereafter referred to as **Zjj**) and on inclusive W production at $\sqrt{s} = 7$ TeV, where experimental data are not yet available, and Zjj, Wjj, inclusive Z, and inclusive W production at $\sqrt{s} = 13$ TeV are also considered.

Unlike a four-jet final state, it has been shown [44,45] that higher-order contributions from single parton scattering (SPS) are crucial for a consistent description of DPS-sensitive observables in the Wjj channel. These are not included in the matrix element simulated by the PYTHIA event generator. Their neglect will lead to incorrect results, and strong disagreement with experimental data. Other event generators, like MADGRAPH [53] and POWHEG [54], which simulate multileg and higher-order matrix elements, are more suitable for studies of the Wjj and Zjj final states. The MADGRAPH event generator includes both NLO and NNLO real corrections to inclusive W and Z processes but no virtual ones, while POWHEG generates a full NLO calculation of Wjj and Zjj cross sections with both real and virtual corrections. The matrix elements generated by MADGRAPH and POWHEG at the parton level are then interfaced to the UE simulation provided by PYTHIA 8. In particular, the applied UE simulation uses the parameters of the so-called "UE Tune" [52], extracted from UE data in hadronic events at transverse scales between 2 and 5 GeV. Even though the hard scales are much higher than 5 GeV in inclusive W- and Z-boson events, our model-independent calculation of σ_{eff} in Wjj and Zjj final states shows values which are very similar to σ_{eff} obtained in the four-jet channel. This looks, however, like a pure numerical coincidence but motivates the choice of using the "UE Tune" also for W- and Z-boson events. However, it is important to note that the value of the reweighting function R in Eq. (1) calculated for Wjj and Zjj is very different from the corresponding reweighting function R for four-jet final states. It is only the ratio between $\sigma_{\text{eff}}^{(0)}$ and R that is numerically similar between the Wjj, Zjj, and four-jet processes.

The paper is organized in the following way. In Sect. 2, the basic formalism and the numerical calculation of σ_{eff} is described, along with its MC implementation. In Sect. 3, predictions of observables on Wjj and Zjj final states are compared for different settings of the UE simulation, while Sect. 4 considers variables on inclusive W and inclusive Z processes. Section 5 shows predictions of variables in the same previous final states at 13 TeV, while summary and conclusions are given in Sect. 6. Theoretical dependence of σ_{eff} in Wjj and Zjj as a function of the dijet transverse scale is investigated in Appendix 1 for 7 and 13 TeV center-of-mass energies, while, in Appendix 2, results obtained with the MADGRAPH MC event generator are considered.

[1] The possibility that initial conditions at low momentum scale Q_0 are not factorized will be discussed elsewhere but a preliminary investigation shows that this effect is numerically small and thus can be neglected.

2 Basic formalism

2.1 Theoretical tools

The approach of the paper is based on the calculation of the MPI cross section by means of the effective cross section $\sigma_{\rm eff}$. In the case of Wjj or Zjj channels, the MPI cross section can be written as

$$\frac{d\sigma^{\rm Wjj/Zjj}}{dt_{12}dt_{34}} = \frac{d\sigma^{\rm W/Z}}{dt_{12}}\frac{d\sigma^{\rm dijet}}{dt_{34}} \times \frac{1}{\sigma_{\rm eff}}, \tag{2}$$

where partons 1 and 2 create the gauge boson, and partons 3 and 4 the dijet system. The pQCD calculation leads to the following expression for $\sigma_{\rm eff}$ in terms of two-particle GPD:

$$\begin{aligned}\frac{1}{\sigma_{\rm eff}} \equiv \int \frac{d^2\mathbf{\Delta}}{(2\pi)^2}[\,&{}_{[2]}GPD_2(x_1, x_3, Q_1^2, Q_2^2; \mathbf{\Delta})_{[2]}\\ &\times GPD_2(x_2, x_4, Q_1^2, Q_2^2; -\mathbf{\Delta})\\ &+{}_{[1]}GPD_2(x_1, x_3, Q_1^2, Q_2^2; \mathbf{\Delta})_{[2]}G(x_2, x_4, Q_1^2, Q_2^2; -\mathbf{\Delta})\\ &+{}_{[1]}GPD_2(x_2, x_4, Q_1^2, Q_2^2; \mathbf{\Delta})_{[2]}GPD_2(x_1, x_3, Q_1^2, Q_2^2; -\mathbf{\Delta})].\end{aligned} \tag{3}$$

The scale $Q_1$of first hard collision is kept fixed to $Q_1 = M_W/2$ and $Q_1 = M_Z/2$ for, respectively, Wjj and Zjj production. The second and third terms in Eq. (3) correspond to the $1 \otimes 2$ mechanism, when two partons are generated from the splitting of a parton at a hard scale after evolution. The first term corresponds to the conventional case of two partons evolving from a low scale, namely the $2 \otimes 2$ mechanism and can be calculated in the mean-field approximation [19–22]. The momentum Δ is conjugated to the relative distance between the two participating partons. The full double GPD is a sum of two terms:

$$\begin{aligned}&GPD_2(x_1, x_3, Q_1^2, Q_2^2, \Delta)\\ &\quad =_{[1]} GPD_2(x_1, x_3, Q_1^2, Q_2^2, \Delta)\\ &\qquad +_{[2]} GPD_2(x_1, x_3, Q_1^2, Q_2^2, \Delta).\end{aligned} \tag{4}$$

Here ${}_{[2]}GPD_2$ corresponds to the part of the GPD$_2$, referring to the occurrence when both partons are evolved from an initial nonperturbative scale. The ${}_{[1]}GPD_2$ function corresponds to the case when one parton evolves up to some hard scale, at which it then splits into two successive hard partons, each of them participating in turn to the hard dijet event.[2]

The difference with respect to [52] is that the partons 1 and 2 are quarks in the case of W- and Z-boson events (u and $\bar{d}$ for W and $u\bar{u}$ or $d\bar{d}$ for Z production), instead of gluons in the case of four-jet final states. Hence, the GPD in Wjj and Zjj is defined as

$$\begin{aligned}&{}_{[2]}GPD_2(x_1, x_3, Q_1^2, Q_2^2, \Delta)\\ &\quad = D_q(x_1, Q_1)D_g(x_3, Q_2)F_{2q}(\Delta, x_1)F_{2g}(\Delta, x_3),\end{aligned} \tag{5}$$

where $D(x, Q^2)$ is a conventional parton distribution function (PDF). The use of the mean-field approximation results in

$$\begin{aligned}&{}_{[2]}GPD_2(x_1, x_3, Q_1^2, Q_2^2, \Delta)\\ &\quad = GPD_q(x_1, Q_1^2, \Delta)GPD_g(x_3, Q_1^2, \Delta),\end{aligned} \tag{6}$$

and

$$GPD_{q,g}(x, Q^2, \Delta) = D_{q,g}(x, Q)F_{2g,2q}(\Delta, x). \tag{7}$$

In the considered processes, the characteristic values of x_i, with $i = 1, ..., 4$ refer to production at central rapidities; hence, there is no need to include conditions such $x_1 + x_3 < 1$ or $x_2 + x_4 < 1$ in Eq. (6) (for a discussion of such kinematic constraints, see e.g. [25]).

The numerical analysis of HERA data shows that the gluonic and quark radii of the nucleon are of similar size [55]. Hence, here we neglect the difference between the two-gluon form factors and its quark analogs. By assuming no difference between the initial partons, the structure functions cancel out in the mean-field calculation of $\sigma_{\rm eff}$. Consequently, the $2 \otimes 2$ part of the calculation can be done using the two-gluon form factors only. For the two-gluon form factor F_{2g}, we use the exponential parametrization described in [21]. In fact, it leads to the same numerical results as the dipole form [19,20], but it is more convenient for calculations. This parametrization is unambiguously fixed by J/Ψ diffractive charmonium photo/electro production at HERA. The functions D are the conventional nucleon structure functions and F_{2g} can be parameterized as

$$F_{2g}(\Delta, x) = \exp(-B_g(x)\Delta^2/2), \tag{8}$$

where $B_g(x) = B_0 + 2K_Q \cdot \log(x_0/x)$, with $x_0 \sim 0.0012$, $B_0 = 4.1$ GeV^{-2}, and $K_Q = 0.14$ GeV^{-2}. In our implementation the central values of the parameters B_0 and K_Q [21] have been used, which are known with an accuracy of $\sim$8 %. Integrating over Δ^2, we obtain for the part of $\sigma_{\rm eff}$ corresponding to the first term in Eq. (3)

$$\frac{1}{\sigma_{\rm eff}^{(0)}} = \frac{1}{2\pi}\frac{1}{B_g(x_1) + B_g(x_2) + B_g(x_3) + B_g(x_4)}, \tag{9}$$

where x_{1-4} are the longitudinal momentum fractions of the partons participating in the $2 \otimes 2$ mechanism. This cross section corresponds to the free parton model and is model independent in the sense that its parameters are determined not from a fit to experimental LHC data but from a fit to single parton GPD. The maximum transversality kinematics for the dijet system, i.e. $4Q^2 = x_3x_4s$, have been considered in

[2] We refer the reader to [22,23] for the detailed definitions of ${}_{[1]}GPD_2$ and ${}_{[2]}GPD_2$ and their connection to nucleon light cone wave functions.

our approach, being Q the dijet transverse scale, and x_3, x_4 the Bjorken fractions of the two jets. Concerning the dependence of $\sigma_{\rm eff}$ on the parton scales, the results documented in [25] show that reweighting factors R in Eq. (9) are different for different final states, e.g. four-jet, Wjj, and Zjj. Hence, we calculated the reweighting factors separately for the two considered channels, Wjj and Zjj. More details on the obtained values of $\sigma_{\rm eff}$ as a function of the dijet scale are described in Appendix 2.

2.2 Monte Carlo implementation and definition of experimental observables

The standard simulation of MPI implemented in PYTHIA 8.205 [39] is considered, but with values of $\sigma_{\rm eff}$ calculated by using the QCD-based approach of [22–25], i.e. including $1 \otimes 2$ processes.

The simulation of the MPI in PYTHIA is based on [38,39]. The PYTHIA code uses single parton distribution functions, dependent on the impact parameter between the two colliding partons. From a theoretical point of view, these are just GPD_1 (see e.g. [56,57] for a review). The parameters set in the PYTHIA simulation relative to the transverse parton density are extracted from fits to experimental data on UE, sensitive to the contribution of the MPI. This procedure is closely related to mean-field-based schemes; see e.g. [22].

The approach developed in [52] and used in the present paper combines the standard PYTHIA MPI model with the one of [22–25]. We use a single gaussian to model the matter distribution function of the protons. With these settings, the value of $\sigma_{\rm eff}^{(0)}$ would be constant and independent of the scale. In order to implement the $\sigma_{\rm eff}$ dependence as a function of the parton momentum fraction x and of the scale, the events from a standard PYTHIA 8 sample, where a hard MPI occur, are reweighted on an event-by-event basis, according to the following relation:

$$w = (1 + R) \cdot \frac{\sigma_{\rm eff}^{(\text{UE Tune})}}{\sigma_{\rm eff}^{(0)}} \tag{10}$$

where w is the applied event weight, $\sigma_{\rm eff}^{(0)}$ and R are the quantities introduced in Eqs. (1) and (9), respectively, and $\sigma_{\rm eff}^{(\text{UE Tune})}$ is the value of $\sigma_{\rm eff}$ predicted by the standard PYTHIA 8 sample. Two types of simulations are considered: one based on the new approach defined in Sect. 1 and called "Dynamic $\sigma_{\rm eff}$", and one which follows the standard PYTHIA 8 approach without any reweighting, called "UE Tune".

The UE Tune [52] has been extracted from fits to UE data in hadronic final states for scales of the leading charged particle in the range 2–5 GeV^2 and its parameters are listed in Table 1.

The first parameter, MultipartonInteractions:pT0Ref, refers to the value of transverse momentum, $p_{\rm T}^0$, defined at $\sqrt{s} = 7$ TeV, used for the regularization of the cross section in the infrared limit, according to the formula $1/p_{\rm T}^4 \to 1/(p_{\rm T}^2 + p_{\rm T}^{0\,2})^2$. The second parameter is the probability of color reconnection among parton strings. The value of $\sigma_{\rm eff}$ is found to be around 29.7 mb at 7 TeV and is quite close to the one determined in the mean-field approach [22,25]. The value of the energy-scaling power ecmPow is taken from Tune 4C [39], which was determined with data measured at 7 TeV and 900 GeV.[3]

Table 1 PYTHIA Eight parameters obtained after the fit to the UE observables

PYTHIA 8 parameter	Value obtained for the UE Tune
MultipartonInteractions:pT0Ref	2.659
ColourReconnection:range	3.540
MultipartonInteractions:ecmPow	0.19
MultipartonInteractions:ecmRef	7000
$\sigma_{\rm eff}$ (7 TeV) (mb)	29.719
$\sigma_{\rm eff}$ (13 TeV) (mb)	31.851

The value of pT0Ref is given at the reference energy of 7 TeV. The parameter ecmPow has been kept fixed to the value used in Tune 4C [39]. Values of $\sigma_{\rm eff}$ at 7 and 13 TeV are also shown in the table

Two different sets of observables are studied in final states with W- or Z-bosons: the first one consists of variables sensitive to hard MPI, the second one includes observables which are mostly influenced by the UE, namely by MPI at moderate scales. Final states with a Z- or a W-boson are separately investigated at the stable-particle level by using the RIVET framework [58]. For the UE study, an inclusive Z- or W-boson production is required. The Z-boson is reconstructed through its muonic decay: two muons with $p_{\rm T} > 20$ GeV in $|\eta| < 2.4$ are required with an invariant mass between 81 and 101 GeV^2. For the W-boson selection, a final state with one muon with $p_{\rm T} > 30$ GeV and $|\eta| < 2.1$ and a missing transverse energy of 30 GeV is required. In the Wjj and Zjj channel, two jets clustered with the anti-$k_{\rm T}$ algorithm with $p_{\rm T} > 20$ GeV in $|\eta| < 2.0$ are added to the selection of, respectively, the W- and the Z-boson. The various final states for which the considered predictions are tested are summarized in Table 2.

The following observables are investigated for the study of DPS in the Wjj and Zjj final states:

$$\Delta \mathrm{S} = \arccos\left(\frac{\mathbf{p}_T(\text{boson}) \cdot \mathbf{p}_T(\text{jet}_{1,2})}{|\mathbf{p}_T(\text{boson})| \times |\mathbf{p}_T(\text{jet}_{1,2})|}\right), \tag{11}$$

$$\Delta^{\rm rel} p_{\rm T} = \frac{|\mathbf{p}_T^{\text{jet}_1} + \mathbf{p}_T^{\text{jet}_2}|}{|\mathbf{p}_T^{\text{jet}_1}| + |\mathbf{p}_T^{\text{jet}_2}|}, \tag{12}$$

[3] If one takes the ecmPow value from more recent tunes, e.g. Tune CUETP8M1 [51], no significant changes in the distributions and in the values of $\sigma_{\rm eff}$ at 13 TeV are observed.

Table 2 Summary of the various selections applied in the W- and Z-boson final states, for studies of UE- and DPS-sensitive observables

FINAL- STATE SELECTION	W-boson	Z-boson
UE selection	Exactly 1 μ: $p_{\mathrm{T}} > 30$ GeV in $\|\eta\| < 2.1$	2 μ: $p_{\mathrm{T}} > 20$ GeV in $\|\eta\| < 2.0$
	$\mathrm{E}_T^{miss} > 30$ GeV and $\mathrm{m}_T^W > 50$ GeV	$\mathrm{m}_{inv}^{\mu\mu}$ in [81,101] GeV^2
DPS selection	Exactly 1 μ: $p_{\mathrm{T}} > 30$ GeV in $\|\eta\| < 2.1$	2 μ: $p_{\mathrm{T}} > 20$ GeV in $\|\eta < 2.0$
	$\mathrm{E}_T^{miss} > 30$ GeV and $\mathrm{m}_T^W > 50$ GeV	$\mathrm{m}_{inv}^{\mu\mu}$ in [81,101] GeV^2
	2 j: $p_{\mathrm{T}} > 20$ GeV in $\|\eta\| < 2.0$	2 j: $p_{\mathrm{T}} > 20$ GeV in $\|\eta\| < 2.0$

where the boson may be the W- or Z-boson, $\mathrm{jet}_{1,2}$ is the jet pair and jet_1 (jet_2) is the leading (subleading) jet.

The study of the UE contribution has been performed through the usual à-la-Rick-Field strategy [59]. The direction of the reconstructed boson identifies the direction of the hard scattering and defines different regions in the plane transverse to the beam direction: the "toward" region ($|\Delta\phi| < 60°$), two transverse regions ($60 < |\Delta\phi| < 120°$) and the "away" region ($|\Delta\phi| > 120°$). Only observables measured in the toward and transverse regions have been considered in this study, since they are the ones which are most affected by the UE contribution. Note that for W and Z production, unlike in hadronic events, the toward region is also sensitive to UE contributions since the decay products of the weak bosons are not counted in the event activity. The observables refer to the amount of number of charged particles and of their transverse momentum and are:

- charged-particle multiplicity density (N_{ch});
- transverse momentum sum density (Σp_{T}).

Charged particles which contribute to these quantities are selected in each event within a region of pseudorapidity $|\eta| < 2.5$ with a lower p_{T} cut of 500 MeV.

The x and scale dependence of σ_{eff} has been implemented in the considered predictions by reweighting on an event-by-event basis the MC simulation in the presence of a hard MPI ($p_{\mathrm{T}} > 15$ GeV). The x dependence is given by Eq. (9), where $x_{1,2}$ are taken as the longitudinal momentum fractions of the partons participating in the hardest scattering (W- or Z-boson production), while $x_{3,4}$ refer to the longitudinal momentum fractions of the partons participating in the hardest MPI. The scale dependence is expressed by Eq. (1), where R takes for Q_2 the scale of the hardest MPI. Different values of Q_0^2 have been considered in the range between 0.5 and 1 GeV^2. Predictions with the following simulation settings are considered for comparison:

- "UE Tune" [52]: predictions obtained without applying any reweighting of the simulation; this tune uses a constant value of σ_{eff}, following the standard PYTHIA approach, and its parameters have been extracted by fits to the UE measurement in hadronic final states;
- "UE Tune x-dep": predictions obtained with the parameters of the UE Tune and by applying the x dependence of σ_{eff};
- "UE Tune Dynamic σ_{eff}": predictions obtained with the parameters of the UE Tune and by applying both x and scale dependence for σ_{eff} values; two different tunes are shown, corresponding to values of Q_0^2 equal to 0.5 and 1 GeV^2. As it was done in four-jet final states [52], the dependence of the cross section on the p_T of the outgoing partons is assumed to be the same in $2 \otimes 2$ and $1 \otimes 2$ production mechanisms. This might affect differential distributions as a function of the jet balance, i.e. $\Delta^{\mathrm{rel}} p_{\mathrm{T}}$.

This approach is implemented for various Monte Carlo event generators which use different matrix-element calculations:

- PYTHIA 8 [37], which implements a 2→2 LO ME ($q\bar{q} \to$ Z and $q\bar{q}' \to$ W for, respectively, Z- and W-boson production), where additional hard partons in the final state are generated through the parton-shower simulation in a leading-log approximation;
- POWHEG [54] interfaced to PYTHIA 8, which implements a 2→4 NLO ME;
- MADGRAPH [53] interfaced to PYTHIA 8, which implements a 2→4 LO ME, where up to four partons in addition to the Z- or the W-boson are simulated within the ME calculation.

The PYTHIA 8 sample uses the CTEQ6L1 [60] PDF set, while the POWHEG sample has been generated with the CT10NLO [61] PDF set. For the MADGRAPH sample, the CTEQ6L1 [60] PDF set has been used and the matching and merging scale between matrix element (ME) and parton shower (PS) have been set to, respectively, 10 and 20 GeV in the MLM formalism [62]. Predictions obtained with the considered event generators have been compared to the ΔS and $\Delta^{\mathrm{rel}} p_{\mathrm{T}}$ observables, measured at 7 TeV by the CMS experiment in the Wjj channel [45] and they are shown in Fig. 2. Predictions obtained with POWHEG and MADGRAPH interfaced to PYTHIA 8 UE Tune follow the shape of the measured points, while PYTHIA 8 does not describe at the same level of the agreement. In particular, higher-order contributions fill the region of the phase space which is most sensitive to the DPS

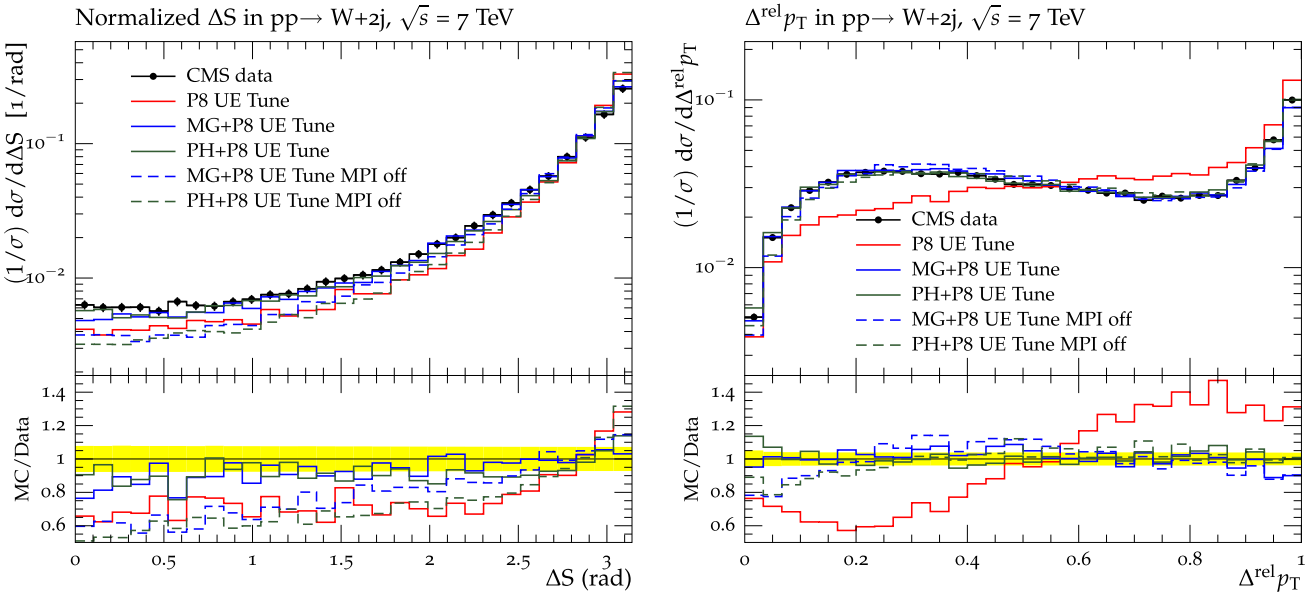

Fig. 2 CMS data [45] at 7 TeV for the normalized distributions of the correlation observables ΔS (*left*) and $\Delta^{\text{rel}} p_{\text{T}}$ (*right*) in the W+dijet channel, compared to predictions generated with PYTHIA 8 UE Tune, MADGRAPH and POWHEG interfaced to PYTHIA 8 UE Tune. Predictions obtained with MADGRAPH and POWHEG interfaced to PYTHIA 8 UE Tune, without the simulation of the MPI are also compared to the measurement. The ratios of these predictions to the data are shown in the *lower panels*

signal. This effect, already observed in [45], is a clear indication of the need of higher-order matrix elements to give a reasonable description of DPS-sensitive observables. Predictions obtained with POWHEG and MADGRAPH without the simulation of MPI, also shown in Fig. 2, are not able to follow the trend of the measured ΔS and $\Delta^{\text{rel}} p_{\text{T}}$. In particular, they underestimate the region of $\Delta\text{S} < 2$ by about 50–70 % and the region of $\Delta^{\text{rel}} p_{\text{T}} < 0.15$ by about 10–20 %. These are the regions of the phase space where a signal from hard MPI is expected to contribute. The large discrepancy observed between data and predictions without the simulation of MPI clearly indicates the need of MPI contributions in the current models for a good description of DPS-sensitive observables.

In the following sections, results are shown by using the POWHEG event generator interfaced to PYTHIA 8, which consistently includes both real and virtual NLO corrections for hard Wjj and Zjj processes. Comparisons with simulations obtained with MADGRAPH, which was used for experimental extractions of σ_{eff} by the CMS collaboration [45], are documented in Appendix 1, while predictions with PYTHIA 8 standalone are dropped from the discussion.

3 DPS-sensitive observables in W+dijet and Z+dijet final states

In this section, comparisons of various predictions for DPS-sensitive observables in Wjj and Zjj are shown at 7 TeV. In Fig. 3, comparisons to data measured by the CMS experiment [45–47] in the Wjj channel at 7 TeV are considered. They refer to the normalized distributions of the correlation observables ΔS (*left*) and $\Delta^{\text{rel}} p_{\text{T}}$ (*right*). Predictions of POWHEG interfaced to PYTHIA 8 UE Tune are considered with different σ_{eff} dependence applied: no reweighting, only x-dependent σ_{eff} values calculated in mean-field approach, x- and scale-dependent σ_{eff} values with $Q_0^2 = 0.5\ \text{GeV}^2$ and $Q_0^2 = 1\ \text{GeV}^2$.

The inclusion of contributions from $1 \otimes 2$ production mechanisms in the predictions with dynamic σ_{eff} values improves the agreement with the measurement for the ΔS observable. They follow the decreasing shape of the observable better than the predictions obtained with the UE Tune without any reweighting and the UE Tune with only x-dependence applied. The $\Delta^{\text{rel}} p_{\text{T}}$ observable is in good agreement with every prediction, except at values $\Delta^{\text{rel}} p_{\text{T}} < 0.15$, where the curves are above the data by about 10–25 %. This might be due to the fact that in our approach we assume the $\Delta^{\text{rel}} p_{\text{T}}$ dependence of the cross section to be the same in $2 \otimes 2$ and $1 \otimes 2$ production mechanisms. This does not need to be true [22–25]. It would be interesting to study if indeed different assumptions on the differential $1 \otimes 2$ and $2 \otimes 2$ cross sections bring about a significant difference and play a role at low values of $\Delta^{\text{rel}} p_{\text{T}}$. However, this requires additional analytical and numerical work and will be done elsewhere [63]. Also, it would be interesting to study the agreement of the considered predictions for a different scale of the dijet system, different from 20 GeV as in this case.

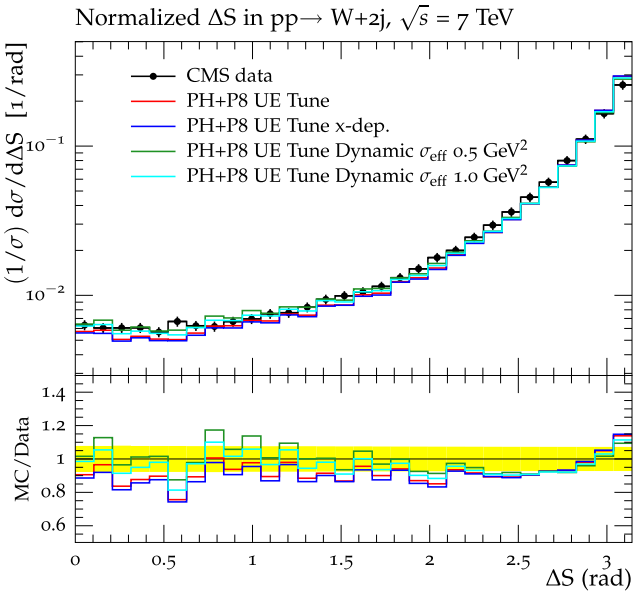

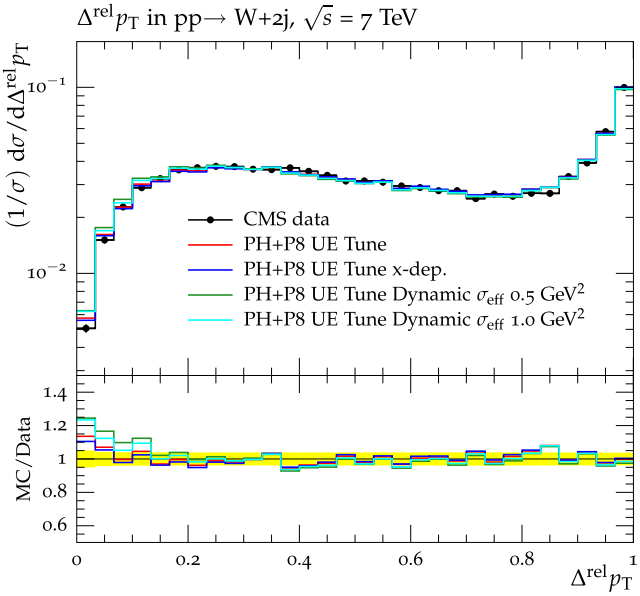

Fig. 3 CMS data at 7 TeV for the normalized distributions of the correlation observables ΔS (*left*) and $\Delta^{\text{rel}}p_{\text{T}}$ (*right*) in the W+dijet channel, compared to predictions of POWHEG interfaced to PYTHIA 8 UE Tune with different σ_{eff} dependence applied: no reweighting applied (*red line*), x-dependent σ_{eff} values (*blue line*), x- and scale-dependent σ_{eff} values with $Q_0^2 = 0.5$ GeV^2 (*green line*) and x- and scale-dependent σ_{eff} values with $Q_0^2 = 1$ GeV^2 (*pink line*). Also shown are the ratios of these tunes to the data

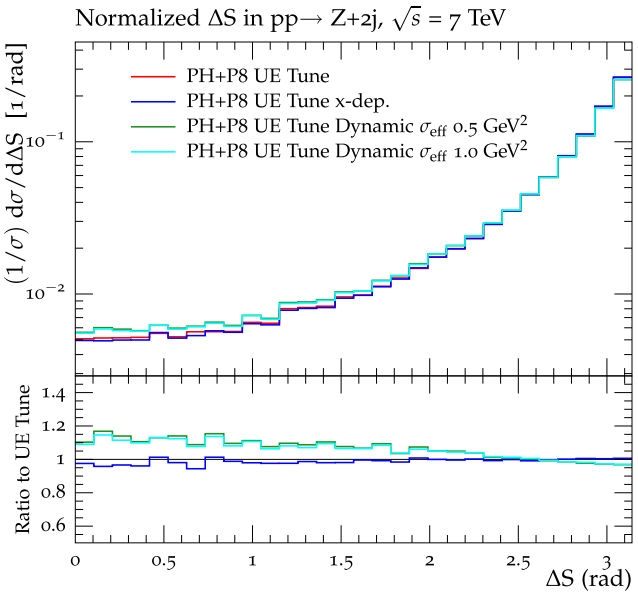

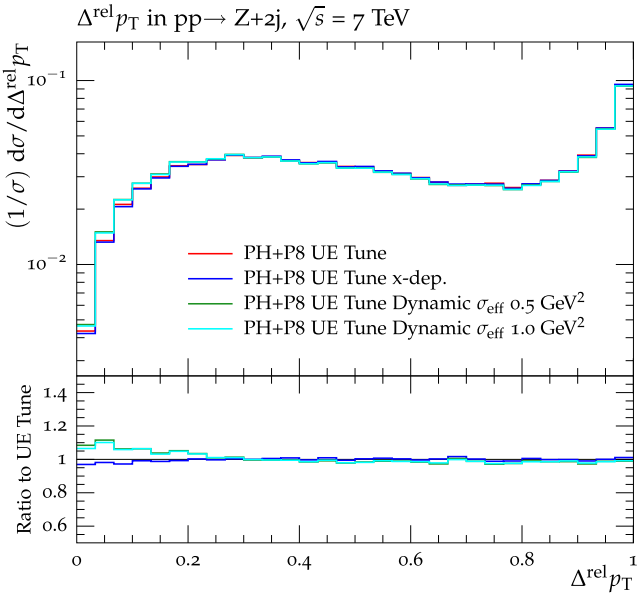

Fig. 4 Predictions at 7 TeV for the normalized distributions of the correlation observables ΔS (*left*) and $\Delta^{\text{rel}}p_{\text{T}}$ (*right*) in the Z+dijet channel, of simulations performed with POWHEG interfaced to PYTHIA 8 UE Tune with different σ_{eff} dependence applied: no σ_{eff} reweighting applied (*red line*), x-dependent σ_{eff} values (*blue line*), x- and scale-dependent σ_{eff} values with $Q_0^2 = 0.5$ GeV^2 (*green line*) and x- and scale-dependent σ_{eff} values with $Q_0^2 = 1$ GeV^2 (*pink line*). Also shown are the ratios of each *curve* to the predictions of the UE Tune

In Fig. 4, predictions obtained with POWHEG interfaced to PYTHIA 8 UE Tune are shown for the normalized distributions of the correlation observables ΔS and $\Delta^{\text{rel}}p_{\text{T}}$ in the Zjj channel. Various simulation settings are considered: no σ_{eff} reweighting applied, UE Tune, x-dependent tune values, x- and scale-dependent xscale tune, with $Q_0^2 = 0.5$ GeV^2, and x- and scale-dependent σ_{eff} values, with $Q_0^2 = 1$ GeV^2. Data points for these observables are not yet measured. Differences among the predictions are of the order of 10–15 % for $\Delta S < 2$ and $\Delta^{\text{rel}}p_{\text{T}} < 0.2$, which are the

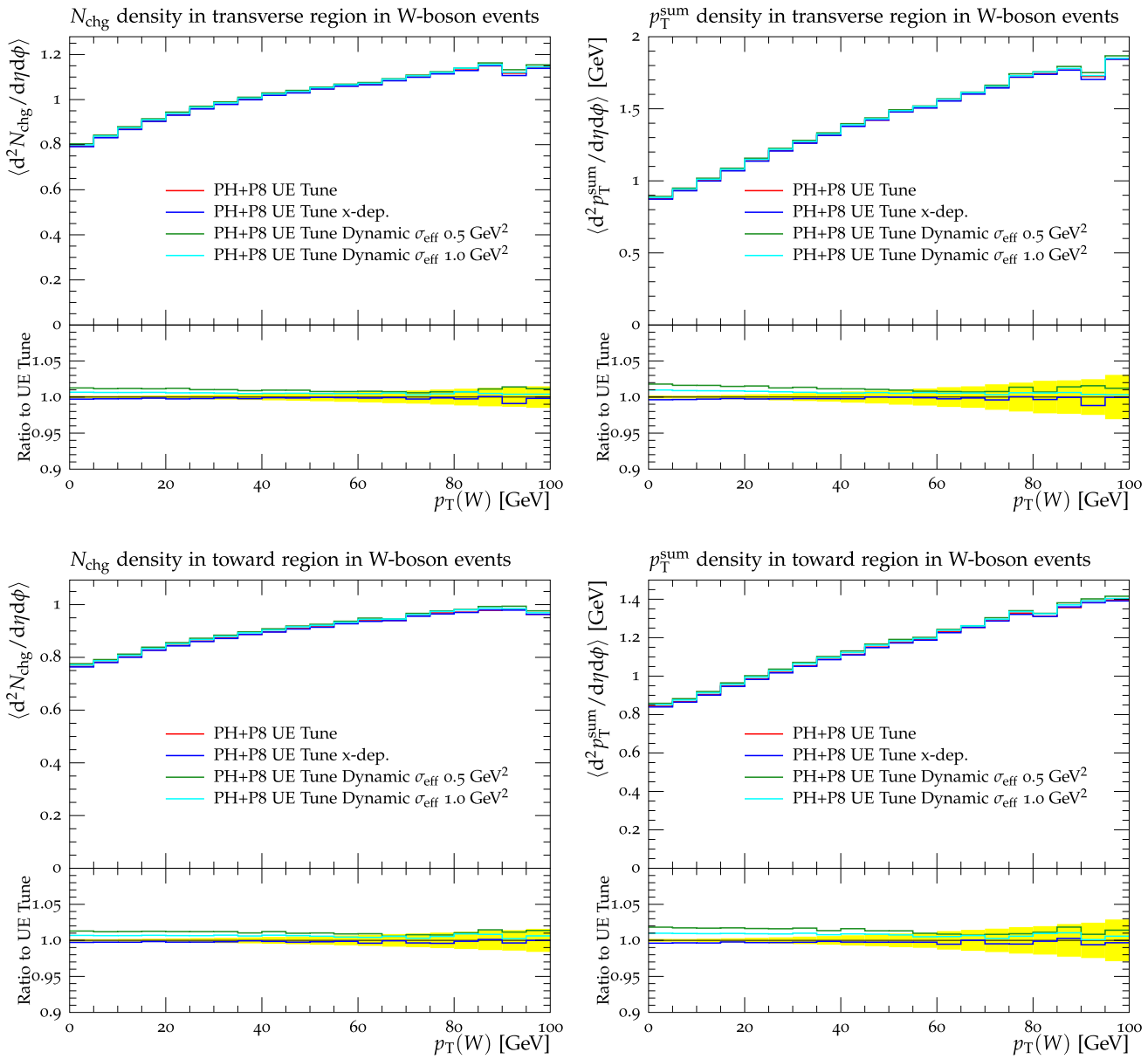

Fig. 5 Predictions for the (*left*) charged-particle and (*right*) p_T sum densities in the transverse (*top*) and toward (*bottom*) regions as defined by the W-boson in proton–proton collisions at 7 TeV. Simulations obtained with POWHEG interfaced to PYTHIA 8 UE Tune are considered with different σ_{eff} dependence applied: no reweighting applied (*red line*), x-dependent σ_{eff} values (*blue line*), x- and scale-dependent σ_{eff} values with $Q_0^2 = 0.5$ GeV^2 (*green line*) and x- and scale-dependent σ_{eff} values with $Q_0^2 = 1$ GeV^2 (*pink line*). Also shown are the ratios of these tunes to the predictions of the UE Tune

regions of the phase space where DPS signals are expected to contribute.

In both W and Z events, the uncertainties due to the knowledge of the parameters of Eq. (9) have been evaluated for all combinations of values within the known parameter uncertainty. A maximal variation of 3–4 % has been observed for the considered DPS-sensitive variables. This value was similar to the one obtained in the four-jet final state [52].

4 UE observables in inclusive W- and Z-boson events

Predictions obtained with the considered tunes are also tested for UE observables in inclusive W- and Z-boson events. This kind of events are sensitive to MPI at moderate scales. In Fig. 5, predictions on charged-particle multiplicity and p_T sum densities are shown for inclusive W events in the transverse and toward regions as a function of the W-boson p_T. Curves obtained with POWHEG interfaced to PYTHIA 8 UE

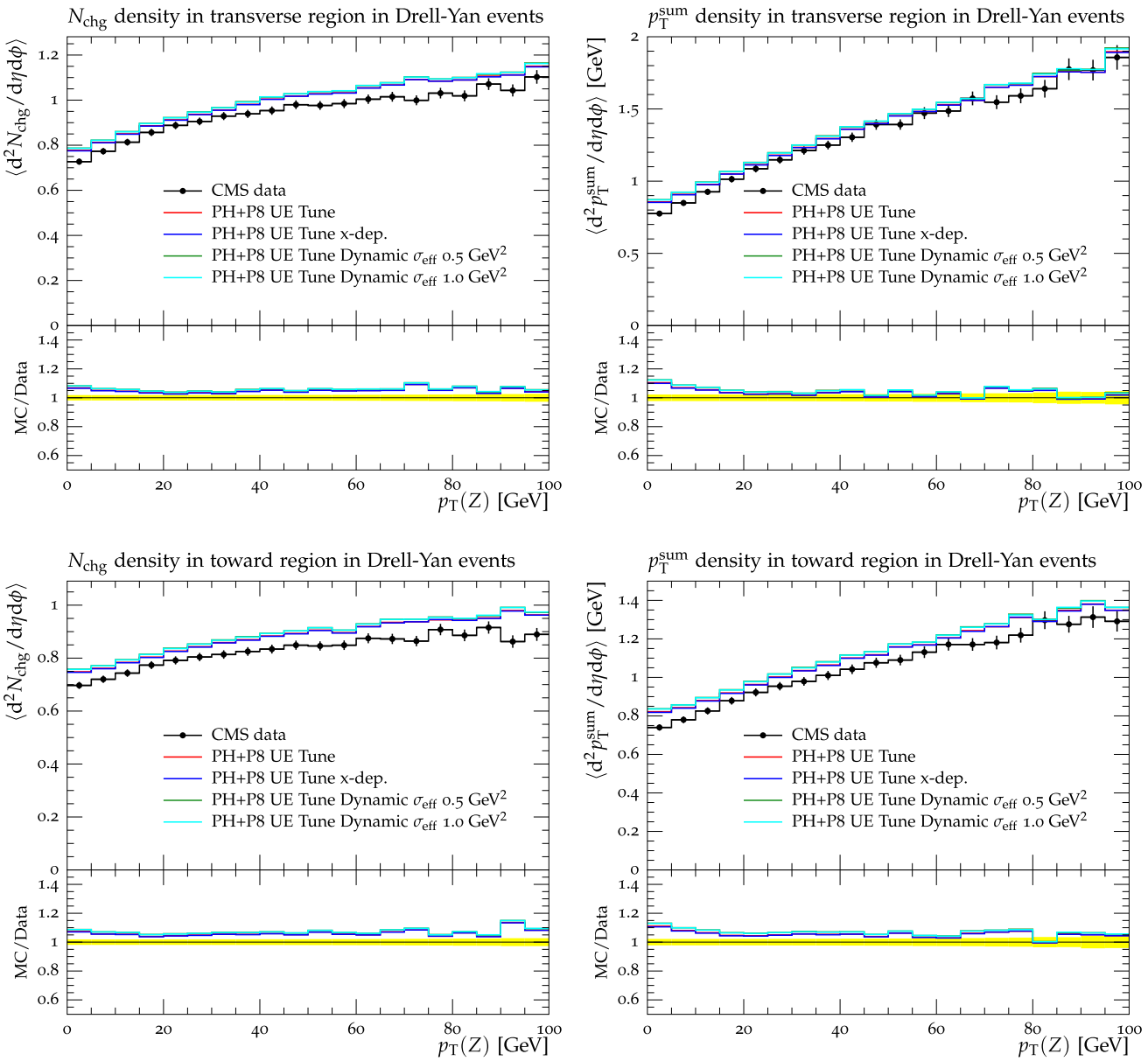

Fig. 6 CMS data [59] for the (*left*) charged-particle and (*right*) p_T sum densities in the transverse (*top*) and toward (*bottom*) region as defined by the Z-boson in Drell–Yan production in proton–proton collisions at 7 TeV. The data are compared to POWHEG interfaced to PYTHIA 8 UE Tune with different σ_{eff} dependence applied: no reweighting applied (*red line*), x-dependent σ_{eff} values (*blue line*), x- and scale-dependent σ_{eff} values with $Q_0^2 = 0.5\,\text{GeV}^2$ (*green line*) and x- and scale-dependent σ_{eff} values with $Q_0^2 = 1\,\text{GeV}^2$ (*pink line*). Also shown are the ratios of these tunes to the data

Tune and implementing different σ_{eff} dependence differ less than 2 % from each other. This effect is very similar to the one observed in hadronic events, documented in [52].

In Fig. 6, various predictions obtained with POWHEG interfaced to PYTHIA 8 UE Tune are shown of the two UE observables in the transverse and toward regions as a function of the Z-boson p_T and compared to the measurement performed by the CMS experiment [59]. As seen in inclusive W events, the difference among the considered curves is of the order of 2 %. All predictions follow the data points reasonably well at all scales, with differences up to 10 %.

For UE observables, the uncertainty in the parameters of Eq. (9) adds a negligible effect on the considered predictions. In conclusion, introducing the contribution of $1 \otimes 2$ mechanisms in the simulation improves the description of measurements of DPS-sensitive observables in Wjj final states. No significant change is observed for variables sensitive to the contribution of moderate MPI, and predictions with or

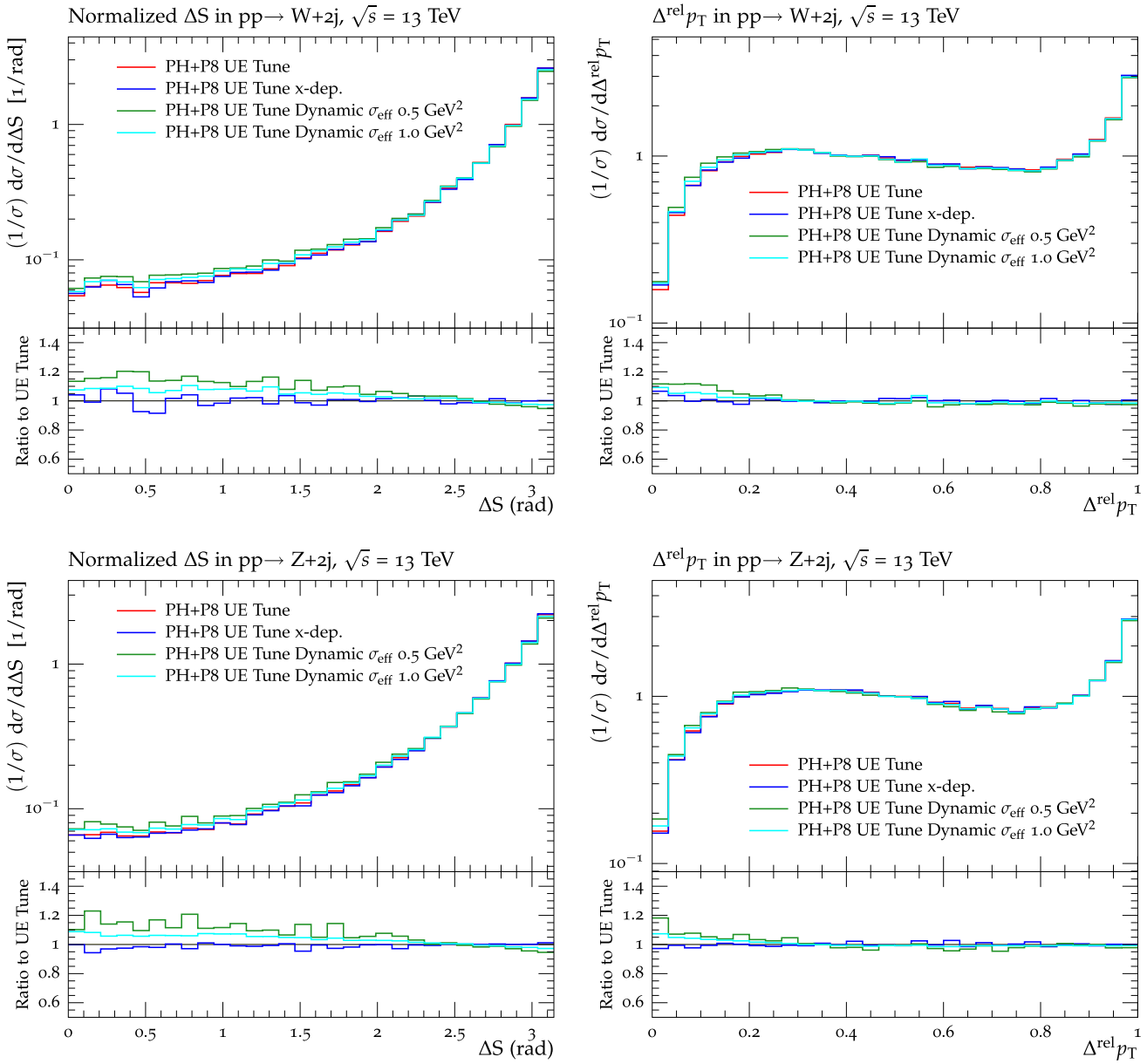

Fig. 7 Predictions at 13 TeV for the normalized distributions of the correlation observables ΔS (*left*) and $\Delta^{\text{rel}} p_{\text{T}}$ (*right*) in the W+dijet (*top*) and Z+dijet *bottom* channels, of simulations performed with POWHEG interfaced to PYTHIA 8 UE Tune with different σ_{eff} dependence applied: no σ_{eff} reweighting applied (*red line*), x-dependent σ_{eff} values (*blue line*), x- and scale-dependent σ_{eff} values with $Q_0^2 = 0.5$ GeV^2 (*green line*) and x- and scale-dependent σ_{eff} values with $Q_0^2 = 1$ GeV^2 (*pink line*). Also shown are the ratios of these tunes to the predictions of the UE Tune

without dynamic σ_{eff} values reproduce the data at the same good level of agreement.

5 Predictions of DPS-sensitive observables at 13 TeV

In this section, predictions of DPS-sensitive observables at 13 TeV are shown for Wjj and Zjj final states. Only the POWHEG event generator is considered with the same settings used for comparisons at 7 TeV. The energy extrapolation of the p_{T}^0 value at 13 TeV is applied through the parameter of the PYTHIA 8 tune 4C [39]. In Fig. 7, predictions at 13 TeV are shown for the normalized distributions of the correlation observables ΔS and $\Delta^{\text{rel}} p_{\text{T}}$ in the Wjj and Zjj channel, obtained with POWHEG interfaced to PYTHIA 8 UE Tune with different σ_{eff} dependence applied: no σ_{eff} reweighting, x-dependent σ_{eff} values, and x- and scale-dependent σ_{eff} values with $Q_0^2 = 0.5$ GeV^2 and $Q_0^2 = 1$ GeV^2. A very sim-

ilar behavior is observed for the two channels. Predictions obtained without any reweighting differ of about 10–15 % from the curves which include the x and scale dependence of $\sigma_{\rm eff}$ in the regions of phase space where a DPS signal is expected to contribute, namely $\Delta S < 2$ and $\Delta^{\rm rel} p_{\rm T} < 0.2$. No relevant difference is observed in the case that a value of Q_0^2 equal to 0.5 or 1.0 GeV^2 is used. A higher DPS sensitivity might result for a different jet selection. For instance, bigger differences, by about 20–25 %, are observed between predictions obtained with POWHEG interfaced toPYTHIA 8 with and without event reweighting, in the case that the two jets are selected with a rapidity separation $\Delta\eta > 6$, in association with a W or a Z-boson. A requirement of a large $|\Delta\eta|$ indeed suppresses the contribution of SPS processes and increases the sensitivity to the DPS contributions.

6 Conclusions

Predictions from the approach developed in [52] for the analysis of multiple parton interactions (MPI) in four-jet final states and including contributions from $1 \otimes 2$ mechanisms, are compatible with measurements sensitive to double parton scattering (DPS) and MPI at moderate scales in W+dijet and Z+dijet channels. This result is highly nontrivial, since, as was stressed in [22–25], the corresponding effective cross section ($\sigma_{\rm eff}$) depends both on the process and on the transverse and longitudinal partonic scales. In order to properly treat events with a W- or a Z-boson with associated jets, it is necessary to include higher-order contributions within the matrix-element calculation. In this paper, simulations using the POWHEG event generator interfaced to the underlying event (UE) simulation provided by PYTHIA 8 are considered. Predictions using dynamic $\sigma_{\rm eff}$ values dependent on the longitudinal momentum fractions and on the scale of the process improve the description of correlation observables measured in W+dijet final states. The experimental accuracy achieved so far does not allow one to draw conclusions as regards the best value of the scale separating soft and hard MPI, Q_0^2. Values of Q_0^2 between 0.5 and 1 describe the measurement at the same level of agreement. Differences by about 15 % are observed between these predictions and measured data if the jet balance in transverse momentum $p_{\rm T}$ ($\Delta^{\rm rel} p_{\rm T}$) is considered. This might be due to the assumption made in our simulation that the differential distributions in the $1 \otimes 2$ mechanisms have the same $p_{\rm T}$ dependence as the conventional $2 \otimes 2$ diagram, as a simple generalization of the formula given in [23–25]. Although explicit formulas for differential distributions of $1 \otimes 2$ production mechanisms are known [24,25], their actual implementation still requires additional work, both analytical and numerical.

An additional issue may be whether the agreement between theory predictions and experimental data can be improved by changes of other parameters in the simulation, such as α_s, or K-factor of SPS production, instead of by the inclusion of $1 \otimes 2$ mechanisms. This task would require additional work which is beyond the scope of this paper. However, a detailed analysis performed in a four-jet final state [50] has showed that tuning additional parameters in the predictions does not lead to an improved description of UE- and DPS-sensitive observables, comparable to the one shown in this paper.

The relevant code, used for the MC simulations in this paper, is publicly available at the following link: http://desy.de/~gunnep/SigmaEffectiveDependence/.

Acknowledgments We thank M. Strikman and H. Jung for very useful discussions and reading the manuscript.

Funded by SCOAP^3.

Appendix A: Results from predictions using MADGRAPH

In this section, we consider results obtained by considering the MADGRAPH event generator. This is interesting to evaluate the contribution of virtual NLO corrections which are included in POWHEG, but not in the calculation of the matrix element implemented in MADGRAPH. Furthermore, the MADGRAPH event generator has been used as reference for the extraction of the DPS contribution in experimental measurements [44–47].

In Fig. 8 (top), measurements from the CMS experiment at 7 TeV of normalized cross sections as a function of ΔS and $\Delta^{\rm rel} p_{\rm T}$ in the Wjj channel are compared to predictions obtained with MADGRAPH interfaced to PYTHIA 8 using various $\sigma_{\rm eff}$ settings. Predictions with a constant value of $\sigma_{\rm eff}$, with x dependence applied and with x and scale dependence applied with $Q_0^2 = 0.5$ and 1.0 GeV^2 are investigated. Predictions with dynamic $\sigma_{\rm eff}$ values dependent on x and on the scale describe better the measurement, especially at values of $\Delta S < 2$ and at $\Delta^{\rm rel} p_{\rm T} < 0.2$. A slightly better agreement than the predictions obtained with the POWHEG matrix element is observed for the normalized cross section as a function of $\Delta^{\rm rel} p_{\rm T}$. As for the POWHEG case, it is not possible to discriminate the best value of Q_0^2, due to the large experimental uncertainty. In Fig. 8 (bottom), predictions with the same settings are tested on ΔS and $\Delta^{\rm rel} p_{\rm T}$ in the Zjj channel. As the results for POWHEG, differences between predictions with dynamic $\sigma_{\rm eff}$ values are 10–15 % above the curve using no $\sigma_{\rm eff}$ reweighting at $\Delta S < 2$ and at $\Delta^{\rm rel} p_{\rm T} < 0.2$.

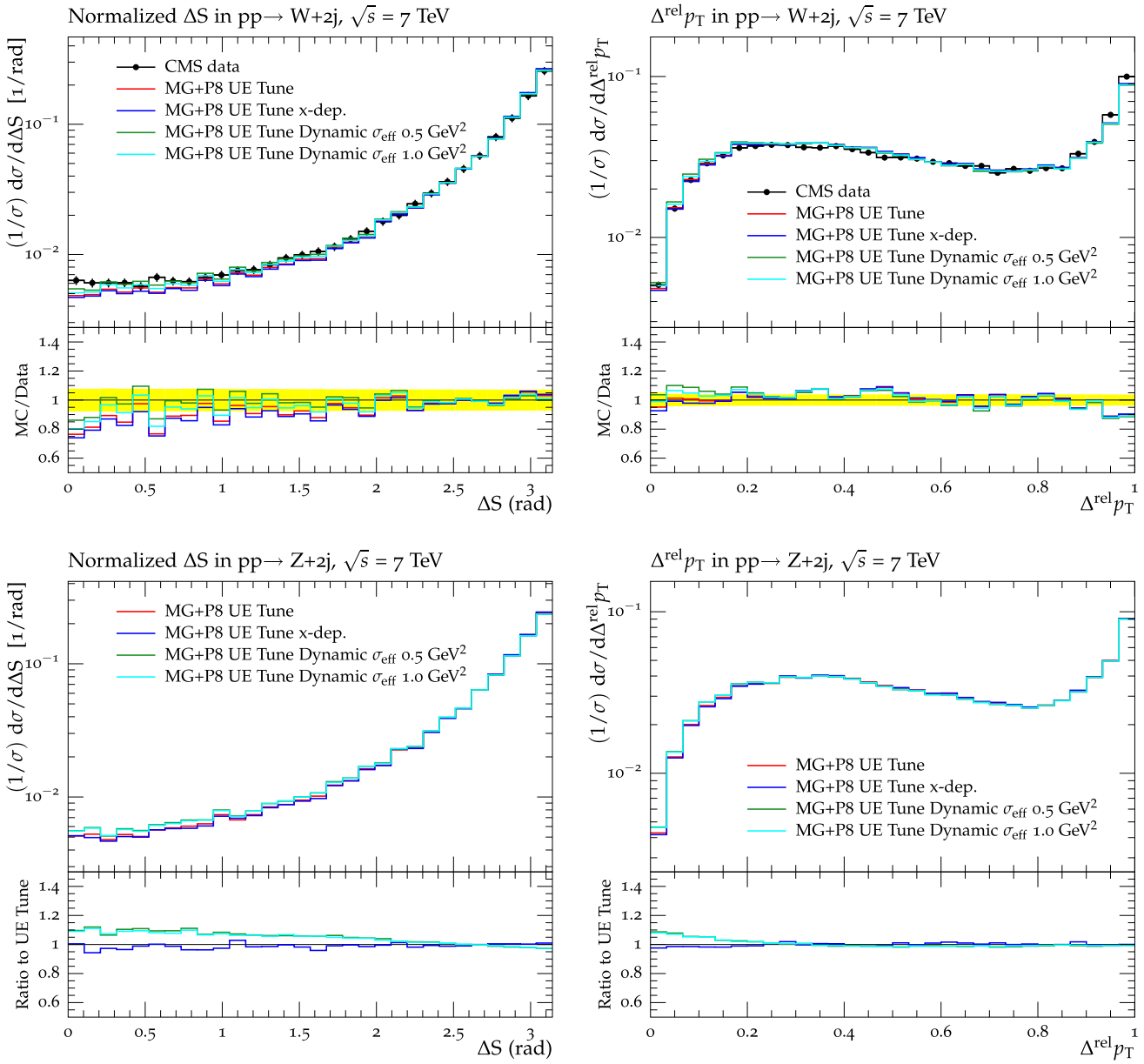

Fig. 8 *Top* CMS data at 7 TeV for the normalized distributions of the correlation observables ΔS (*left*) and $\Delta^{\text{rel}} p_{\text{T}}$ (*right*) in the W+dijet channel, compared to predictions of MADGRAPH interfaced to PYTHIA 8 UE Tune with different σ_{eff} dependence applied: no reweighting applied (*red line*), x-dependent σ_{eff} values (*blue line*), x- and scale-dependent σ_{eff} values with $Q_0^2 = 0.5$ GeV^2 (*green line*) and x- and scale-dependent σ_{eff} values with $Q_0^2 = 1$ GeV^2 (*pink line*). Also shown are the ratios of these predictions to the data. *bottom* Predictions at 7 TeV for the normalized distributions of the correlation observables ΔS (*left*) and $\Delta^{\text{rel}} p_{\text{T}}$ (*right*) in the Z+dijet channel, of simulations performed with MADGRAPH interfaced to PYTHIA 8 UE Tune with different σ_{eff} dependence applied: no σ_{eff} reweighting applied (*red line*), x-dependent σ_{eff} values (*blue line*), x- and scale-dependent σ_{eff} values with $Q_0^2 = 0.5$ GeV^2 (*green line*) and x- and scale-dependent σ_{eff} values with $Q_0^2 = 1$ GeV^2 (*pink line*). Also shown are the ratios of these tunes to the predictions of the UE Tune

In Fig. 9, the observables sensitive to the UE are investigated by comparing different MADGRAPH predictions. In Fig. 9 (top), predictions on the charged-particle multiplicity and p_{T} sum densities as a function of the W-boson p_{T} are shown in the inclusive W channel, while in Fig. 9 (bottom) the same predictions are compared to the CMS measurement in the inclusive Z channel. Very similar conclusions as drawn when considering POWHEG can be extracted. Differences among the various predictions are observed only of the order of 2 % and, in the case of inclusive Z production, all of them reproduce the trend of the measured points.

In conclusion, DPS-sensitive observables are better described by predictions using dynamic σ_{eff} values, while variables

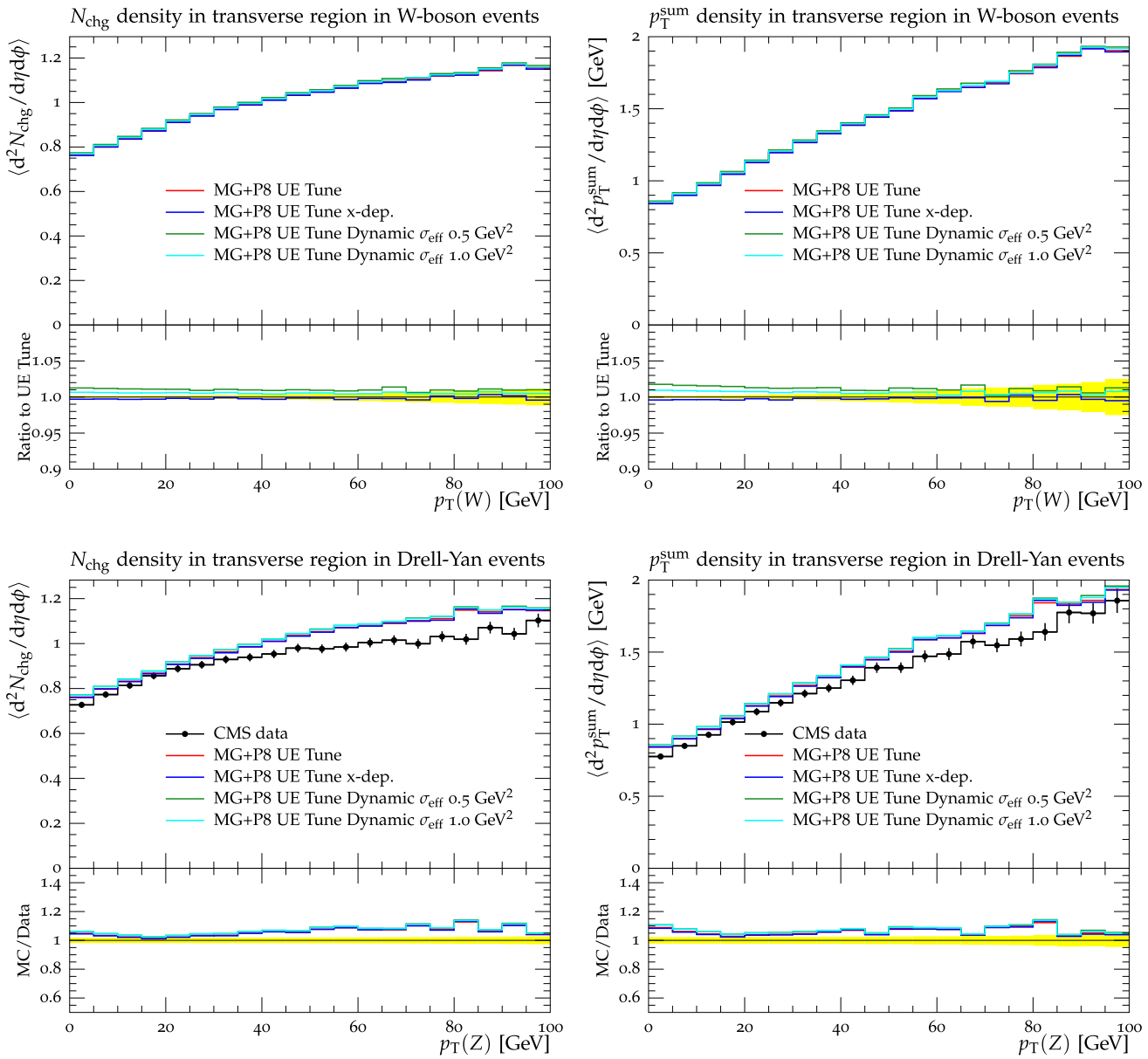

Fig. 9 (*Top*) predictions for the (*left*) charged-particle and (*right*) p_T sum densities in the transverse regions as defined by the W-boson in proton–proton collisions at 7 TeV. Simulations obtained with MADGRAPH interfaced to PYTHIA 8 UE Tune are considered with different σ_{eff} dependence applied: no reweighting applied (*red line*), x-dependent σ_{eff} values (*blue line*), x- and scale-dependent σ_{eff} values with $Q_0^2 = 0.5$ GeV^2 (*green line*) and x- and scale-dependent σ_{eff} values with $Q_0^2 = 1$ GeV^2 (*pink line*). Also shown are the ratios of these tunes to the predictions of the UE Tune. (*bottom*) CMS data for the (*left*) charged-particle and (*right*) p_T sum densities in the transverse region as defined by the Z-boson in Drell–Yan production in proton–proton collisions at 7 TeV. The data are compared to MADGRAPH interfaced to PYTHIA 8 UE Tune with different σ_{eff} dependence applied: no reweighting applied (*red line*), x-dependent σ_{eff} values (*blue line*), x- and scale-dependent σ_{eff} values with $Q_0^2 = 0.5$ GeV^2 (*green line*) and x- and scale-dependent σ_{eff} values with $Q_0^2 = 1$ GeV^2 (*pink line*). Also shown are the ratios of these predictions to the data

sensitive to MPI at moderate scales are not strongly affected by σ_{eff} variation within our approach. This is also the case for POWHEG. Considering the fact that same conclusions hold for MADGRAPH and POWHEG, real NLO corrections are dominant in Wjj and Zjj final states, while virtual ones have a low impact.

Appendix B: Values of sigma effective

In this section, a closer look at the σ_{eff} dependence as a function of collision energy and parton scales is taken. Fig. 10 shows the values of σ_{eff} as a function of the scale of the secondary hard scattering for values of Q_0^2 of 0.5 and 1.0

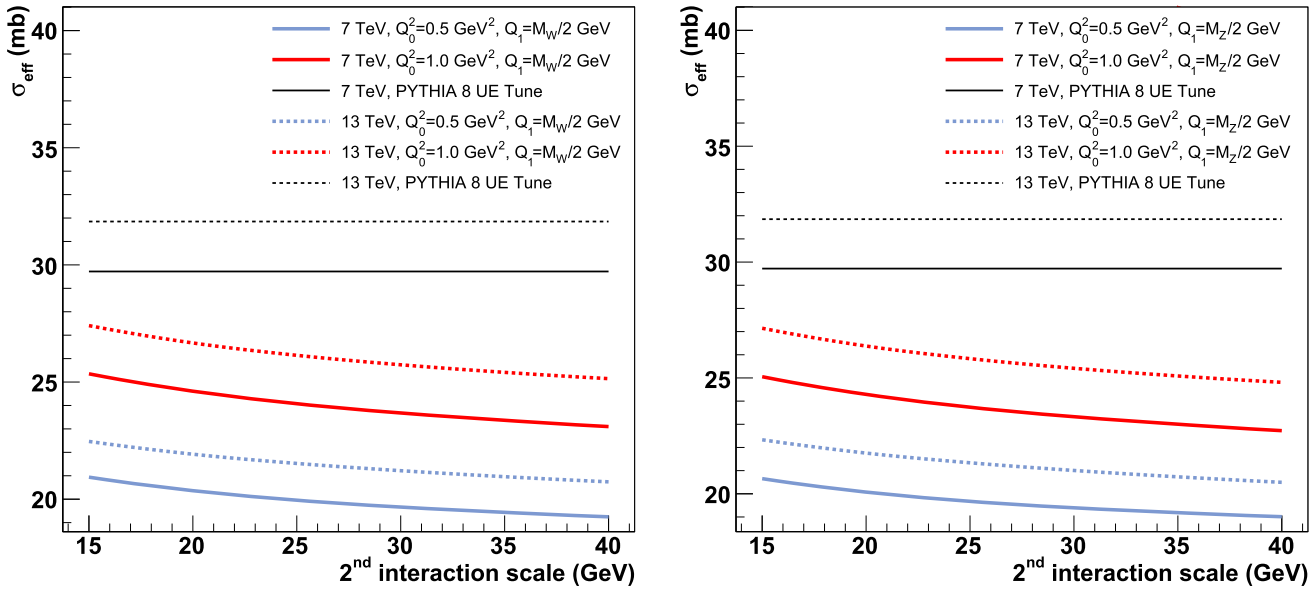

Fig. 10 Values of σ_{eff} as a function of the scale of the second interaction at different collision energies at 7 TeV and 13 TeV for first hard interactions occurring at a scale Q_1 equal to $M_W/2$ and $M_Z/2$ GeV for, respectively, Wjj (*left*) and Zjj (*right*) channels. The two values of Q_0^2 equal to 0.5 and 1.0 GeV^2 are considered and the longitudinal momentum fractions of the two dijets correspond to the maximal transverse momentum exchange for both $\sqrt{s}$ = 7 TeV and $\sqrt{s}$ = 13 TeV. Also shown are the values of σ_{eff} for each energy, as implemented in the PYTHIA 8 UE Tune if no reweighting is applied

GeV^2 at $\sqrt{s} = 7$ and 13 TeV for the considered channels, Wjj and Zjj. The scale of the hard scattering is kept fixed to the maximum of the Breit–Wigner distribution, namely $M_W/2$ and $M_Z/2$ for, respectively, Wjj and Zjj final states. Values of σ_{eff} are slowly decreasing as a function of the scale of the secondary interaction and change of about 1–2 mb between 15 and 40 GeV, independently on the Q_0^2 value. The change in center-of-mass energy brings the value of σ_{eff} up to about 4–5 mb. Similar conclusions can be extracted from the two considered channels.

References

1. N. Paver, D. Treleani, Nuovo Cim. A **70**, 215 (1982)
2. N. Paver, D. Treleani, Z. Phys. C **28**, 187 (1985)
3. M. Mekhfi, Phys. Rev. D **32**, 2371 (1985)
4. R. Kirschner, Phys. Lett. B **84**, 266 (1979)
5. V.P. Shelest, A.M. Snigirev, G.M. Zinovjev, Phys. Lett. B **113**, 325 (1982)
6. A. Del Fabbro, D. Treleani, Phys. Rev. D **61**, 077502 (2000). arXiv:hep-ph/9911358
7. A. Del Fabbro, D. Treleani, Phys. Rev. D **63**, 057901 (2001). arXiv:hep-ph/0005273
8. A. Accardi, D. Treleani, Phys. Rev. D **63**, 116002 (2001). arXiv:hep-ph/0009234
9. S. Domdey, H.J. Pirner, U.A. Wiedemann, Eur. Phys. J. C **65**, 153 (2010). arXiv:0906.4335 [hep-ph]
10. T.C. Rogers, A.M. Stasto, M.I. Strikman, Phys. Rev. D **77**, 114009 (2008). arXiv:0801.0303 [hep-ph]
11. M. Diehl, PoS D **IS2010**, 223 (2010). arXiv:1007.5477 [hep-ph]
12. M. Diehl, A. Schafer, Phys. Lett. B **698**, 389 (2011). arXiv:1102.3081 [hep-ph]
13. M. Diehl, D. Ostermeier, A. Schafer, JHEP **1203**, 089 (2012). arXiv:1111.0910 [hep-ph]
14. E.L. Berger, C.B. Jackson, G. Shaughnessy, Phys. Rev. D **81**, 014014 (2010). arXiv:0911.5348 [hep-ph]
15. M.G. Ryskin, A.M. Snigirev, Phys. Rev. D **83**, 114047 (2011). arXiv:1103.3495 [hep-ph]
16. J.R. Gaunt, W.J. Stirling, JHEP **1003**, 005 (2010). arXiv:0910.4347 [hep-ph]
17. J.R. Gaunt, C.H. Kom, A. Kulesza, W.J. Stirling, Eur. Phys. J. C **69**, 53 (2010). arXiv:1003.3953 [hep-ph]
18. J.R. Gaunt, W.J. Stirling, JHEP **1106**, 048 (2011). arXiv:1103.1888 [hep-ph]
19. L. Frankfurt, M. Strikman, C. Weiss, Phys. Rev. D **69**, 114010 (2004). arXiv:hep-ph/0311231
20. L. Frankfurt, M. Strikman, C. Weiss, Ann. Rev. Nucl. Part. Sci. **55**, 403 (2005). arXiv:hep-ph/0507286
21. L. Frankfurt, M. Strikman, C. Weiss, Phys. Rev. D **83**, 054012 (2011). arXiv:1009.2559 [hep-ph]
22. B. Blok, Yu. Dokshitzer, L. Frankfurt, M. Strikman, Phys. Rev. D **83**, 071501 (2011). arXiv:1009.2714 [hep-ph]
23. B. Blok, Yu. Dokshitser, L. Frankfurt, M. Strikman, Eur. Phys. J. C **72**, 1963 (2012). arXiv:1106.5533 [hep-ph]
24. B. Blok, Y. Dokshitser, L. Frankfurt, M. Strikman. (2016). arXiv:1206.5594v1 [hep-ph] (unpublished)
25. B. Blok, Y. Dokshitzer, L. Frankfurt, M. Strikman, Eur. Phys. J. C **74**, 2926 (2014). arXiv:1306.3763 [hep-ph]
26. J.R. Gaunt, R. Maciula, A. Szczurek, Phys. Rev. D **90**(5), 054017 (2014). arXiv:1407.5821 [hep-ph]
27. J.R. Gaunt, JHEP **1301**, 042 (2013). arXiv:1207.0480 [hep-ph]
28. S. Gieseke, C.A. Rohr, A. Siodmok. (2016). arXiv:1110.2675 [hep-ph]
29. S. Gieseke, D. Grellscheid, K. Hamilton, A. Papaefstathiou, S. Platzer, P. Richardson, C. A. Rohr, P. Ruzicka et al. (2011). arXiv:1102.1672 [hep-ph]

30. M.H. Seymour, A. Siodmok, JHEP **1310**, 113 (2013). arXiv:1307.5015 [hep-ph]
31. S. Gieseke, C. Rohr, A. Siodmok, Eur. Phys. J. C **72**, 2225 (2012). arXiv:1206.0041 [hep-ph]
32. M. Bähr, M. Myska, M.H. Seymour, A. Siodmok, JHEP **1303**, 129 (2013). arXiv:1302.4325 [hep-ph]
33. K. Golec-Biernat, E. Lewandowska, M. Serino, Z. Snyder, A.M. Stasto, Phys. Lett. B **750**, 559–564 (2015). arXiv:1507.08583 [hep-ph]
34. T. Sjostrand, M. van Zijl, Phys. Rev. D **36**, 2019 (1987)
35. J.M. Butterworth, J.R. Forshaw, M.H. Seymour, Z. Phys, C **72**, 637 (1996). arXiv:hep-ph/9601371
36. T. Sjostrand, P.Z. Skands, Eur. Phys. J. C **39**, 129 (2005). arXiv:hep-ph/0408302
37. T. Sjstrand et al., Comput. Phys. Commun. **191**, 159 (2015). doi:10.1016/j.cpc.2015.01.024. arXiv:1410.3012 [hep-ph]
38. R. Corke, T. Sjöstrand, JHEP **1105**, 009 (2011). arXiv:1101.5953 [hep-ph]
39. R. Corke, T. Sjöstrand, JHEP **1103**, 032 (2011). arXiv:1011.1759 [hep-ph]
40. C. Flensburg, G. Gustafson, L. Lonnblad, A. Ster, JHEP **1106**, 066 (2011). arXiv:1103.4320 [hep-ph]
41. F. Abe et al., CDF Collaboration. Phys. Rev. D **56**, 3811 (1997)
42. V.M. Abazov et al., D0 Collaboration. Phys. Rev. D **81**, 052012 (2010)
43. V.M. Abazov et al., D0 Collaboration. Phys. Rev. D **83**, 052008 (2011)
44. G. Aad et al., ATLAS Collaboration. New J. Phys. **15**, 033038 (2013). arXiv:1301.6872 [hep-ex]
45. S. Chatrchyan et al., CMS Collaboration. JHEP **1403**, 032 (2014). arXiv:1312.5729 [hep-ex]
46. S. Chatrchyan et al., CMS Collaboration. JHEP **1312**, 030 (2013). arXiv:1310.7291 [hep-ex]
47. S. Chatrchyan et al., CMS Collaboration, Phys. Rev. D **89**(9), 092010 (2014). arXiv:1312.6440 [hep-ex]
48. CMS Collaboration [CMS Collaboration], CMS-PAS-SMP-14-009
49. CMS Collaboration [CMS Collaboration], CMS-PAS-FSQ-13-010
50. P. Gunnellini, DESY-THESIS-2015-010
51. V. Khachatryan et al., [CMS Collaboration], Eur. Phys. J. C **76**(3), 155 (2016). arXiv:1512.00815 [hep-ex]
52. B. Blok, P. Gunnellini, Eur. Phys. J. C **75**(6), 282 (2015). arXiv:1503.08246 [hep-ph]
53. J. Alwall et al., JHEP **1407**, 079 (2014). arXiv:1405.0301 [hep-ph]
54. J.M. Campbell, R.K. Ellis, P. Nason, G. Zanderighi, JHEP **1308**, 005 (2013). arXiv:1303.5447 [hep-ph]
55. M. Strikman, C. Weiss, Phys. Rev. D **80**, 114029 (2009)
56. M. Diehl, Phys. Rept. **388**, 41 (2003). arXiv:hep-ph/0307382
57. A.V. Belitsky, A.V. Radyushkin, Phys. Rept. **418**, 1 (2005). arXiv:hep-ph/0504030
58. A. Buckley, J. Butterworth, L. Lonnblad, D. Grellscheid, H. Hoeth, J. Monk, H. Schulz, F. Siegert, Comput. Phys. Commun. **184**, 2803 (2013). arXiv:1003.0694 [hep-ph]
59. S. Chatrchyan et al., CMS Collaboration. JHEP **1109**, 109 (2011). arXiv:1107.0330 [hep-ex]
60. J. Pumplin, D.R. Stump, J. Huston, H.L. Lai, P.M. Nadolsky, W.K. Tung, JHEP **0207**, 012 (2002). arXiv:hep-ph/0201195
61. H.L. Lai, M. Guzzi, J. Huston, Z. Li, P.M. Nadolsky, J. Pumplin, C.-P. Yuan, Phys. Rev. D **82**, 074024 (2010). arXiv:1007.2241 [hep-ph]
62. J. Alwall et al., Eur. Phys. J. C **53**, 473 (2008). arXiv:0706.2569 [hep-ph]
63. B. Blok, P. Gunnellini. (2016) (in preparation)